IAC–24, C3,IP,16,x81244

Multi-Material 3D Printing of a Magnetron

Anjana Valsalan[a*], Xavier Walls Perez[b], Alex Ellery[c]

[a] *Graduate Student - Department of Mechanical and Aerospace Engineering, Carleton University, Ottawa, Canada, anjanavalsalan@cmail.carleton.ca*
[b] *Department of Mechanical and Aerospace Engineering, Carleton University, Ottawa, Canada, xavierwallsperez@cmail.carleton.ca*
[c] *Department of Mechanical and Aerospace Engineering, Carleton University, Ottawa, Canada, aellery@mae.carleton.ca*
[*] *Corresponding author*

Abstract

Solar Power Satellites face the challenge of extremely high production costs as they require several launches for space-based assembly. 3D printing the parts of Solar Power Satellites in space can reduce these launch costs drastically. The main issue arises when attempting to 3D print technological components such as the cavity magnetron. This paper showcases the design and modelling process for 3D printing a magnetron using conductive materials. The method specifically shows how each part of the cavity magnetron is modelled, simulated and then printed. The initial iteration of the magnetron uses copper due to its high electrical and thermal conductivity required for the operation of the magnetron. Further iterations of the magnetron will be printed in materials that can be obtained from a lunar environment such as aluminium. This paper examines the feasibility of 3D printing the components of a cavity magnetron for use in Solar Power Satellites, as well as the possibility of using lunar materials for 3D printing.

Acronyms/Abbreviations

SPS = Solar Power Satellite
DED = Directed Energy Deposition
L-PBF = Laser-Powder Bed Fusion

1. Introduction

Solar Power Satellites (SPS) are systems capable of providing renewable energy through the process of converting uninterrupted solar energy into a form that can be received on Earth [1]. There are two main methods used for power transmission by SPS systems: laser power beaming and microwaves. Microwave SPS are the systems that this paper is considering. These SPS systems consist of solar cell arrays that convert solar energy into electricity and feed to microwave generators such as a magnetron [2]. The magnetron would then be able to transmit a very low power microwave beam safely to a receiver on Earth via an antenna as seen in Fig.1. This process could potentially supply the world's power grids, allowing for a cleaner more sustainable future.

The issue that arises with implementing SPS system, is the large costs that are required for transporting the satellites in space as well as producing the satellites [2]. These costs could be reduced significantly by making use of lunar resources. Using metal powders made of elements found in the lunar environment can allow the components of the SPS system to be 3D printed, using methods such as Directed Energy Deposition (DED) or Laser-Powder Bed Fusion (L-PBF), in space rather than manufactured on Earth. The challenge then becomes, how the more complex components such as the magnetron could be 3D printed. This paper discusses the initial steps that are being taken to showcase a proof of concept for the 3D printing of a magnetron. First a 3D printed magnetron made of copper would be developed and tested. If this is functional, then an attempt at 3D printing a functional aluminum magnetron would be made. The aluminum magnetron would serve as a proof of concept that lunar materials can be used to 3D print the more complex components within the SPS system.

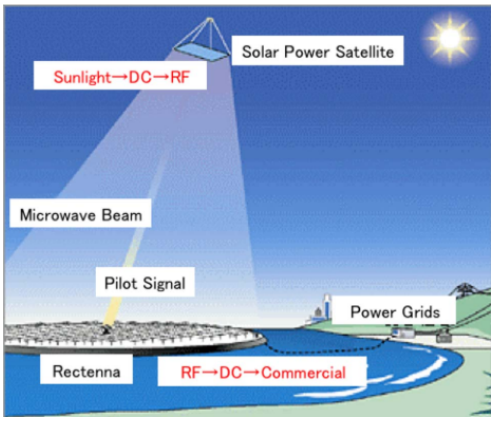

Fig. 1. Representation of an SPS System Using Microwaves [3]

1.1 Magnetron theory of operation

Prior to designing a 3D printed magnetron, the theory of operation needed to be understood. The magnetron oscillator is a Vacuum Tube oscillator that generates microwave signals by transferring energy from an electron stream to a radio frequency (RF) field [4]. The basic structure of the magnetron consists of two main components: the cathode and the anode. The cathode is a cylindrical solid structure that is placed within the anode on its axis. The anode is a cylindrical structure with several cavity resonators. The outer wall of the anode can be considered the inductive element, while the tips of the vanes are the capacitor region. The general arrangement within a magnetron can be seen in Fig. 2.

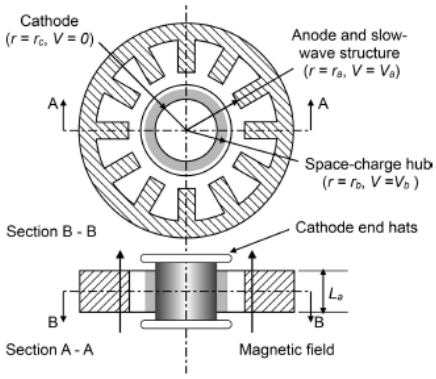

Fig. 2. General Arrangement of a Magnetron [5]

Typically, the magnetron is made using materials such as Copper for the anode and Thoriated Tungsten for the Cathode. These are materials not are not commonly found in large enough quantities in a lunar environment, thus an investigation into whether a magnetron can be made of alternative metals such as aluminum is important for the viability of 3D printing the structures using lunar resources.

In the magnetron, the cathode is heated through a process known as ohmic heating. This causes electrons to be emitted from the cathode and accelerated towards the anode due to the voltage potential established across the anode. The magnetron structure is operated between two strong magnets which establish a strong magnetic field between the anode and cathode. This produces a force that is perpendicular to the DC field on each electron. This causes the electrons to move in a spiral fashion away from the cathode. As the electrons reach the anode, they are influenced by the RF fields at the vanes and either slow down or accelerate depending on the direction of the RF field. Electrons that slow down will move towards the anode while the ones that are accelerated will curl away from the anode [6]. This results in a collection of electrons in a spoke formation near the anode as seen in Figure 3.

Fig. 3. Spoke Formation of Electrons in the Magnetron [6]

The theory of operation was used to ensure that an understanding of what is needed to create a functional magnetron is maintained while creating a design and model. The model designed in this paper takes into account the constraints required for 3D printing processes as well as the required details for proper magnetron operation.

2. Design and modelling process

The steps taken to produce a model of magnetron was to first observe the construction of a magnetron by deconstructing a commercial magnetron that is meant for household microwave ovens, then initial measurements were taken to act as a reference point when performing design calculation. The design calculations were done to obtain design parameters for different aspects of magnetron. The magnetron's performance heavily relies on the measurements of the various components, such as anode height, the number of vanes and the diameter of the interaction space. These parameters were considered before creating a model of the magnetron that could be simulated and then printed.

2.1 Magnetron disassembly

Prior to purchasing a commercial magnetron for deconstruction, verification was needed to ensure that the ceramic seals used in the magnetron did not contain Beryllium Oxide. Beryllium Oxide is a material that was commonly used in the manufacturing of commercial magnetrons and it is highly toxic in a dust form. If the ceramic seals were made of Beryllium Oxide and if they were to break during the disassembly process, it would have been very dangerous. However, the manufacturer was able to verify that the 2M214 continuous wave magnetron did not use Beryllium Oxide and so this was the magnetron that was chosen as a reference.

Fig. 4. Magnetron Tube for the 2M214

The commercial magnetron structure was composed of a steel housing encasing the magnetron vacuum tube. within the housing, the vacuum tube was sandwiched between two ferrite magnets and six aluminum fins. The steel housing was removed along with the capacitor and choke coil in the filter box. The magnets were then removed and put aside for potential use with the 3D printed magnetron. The aluminum cooling fins were removed leaving behind the magnetron tube structure as seen in Fig. 4.

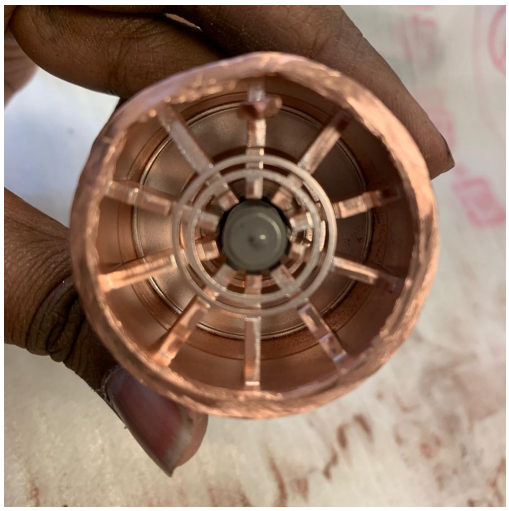

Fig. 5. Cross-Section of the 2M214 Magnetron

The large cylindrical section of the magnetron was separated from the top and bottom ceramic seals allowing the internal structure of the magnetron to be observed. The 2M214 consisted of a 10 vane anode with a filament cathode wrapped around a rod and connected to an endcap. The vanes were connected by two strapping rings which alternated in contact points between the vanes as seen in Fig. 5. The dissected Magnetron was measured for reference dimensions. The noted parameters are shown in Table 1. These parameters were then used as a baseline for the design calculations of the magnetron.

Table 1. 2M214 Physical Parameters

Measured Parameter	Symbol	Value
Anode Outer Rim Radius	$r_{an_{orim}}$	20mm
Anode Inner Radius	$r_{an_{ir}}$	5mm
Anode Height	h	20mm
Number of Vanes	N	10
Vane Length	v_l	12.6mm
Vane Thickness	v_t	2mm
Cathode Radius	r_c	3mm

2.2 Design calculations

The primary design parameters that need to be considered include the frequency, power output and voltage [7]. The commercial magnetron provided frequency, power output and voltage values as being 2.46GHz, 950W and 4.4kV respectively. Rather than designing for the commercially used 2.46GHz frequency used by the commercial magnetron, a 5.8 GHz was chosen instead as discussed in [3]. The measurements for the physical design of the commercial magnetron were used as a basis to begin the design process. While the commercial design used 10 vanes, 8 vanes were chosen to simplify the design. For the design of the 3D printed model, the most basic version of the magnetron was designed. The number of vanes chosen was used to determine the π-mode or non-degenerative mode of the magnetron using (1).

$$n = \frac{N}{2} \quad [1]$$

An initial cutoff static magnetic field, B_0, was found using (2) so as to establish the largest magnetic field that could be applied. The values e and m_0 are the electron charge and the mass of the electron at rest, respectively. The constant e was taken to be $-1.602177 \times 10^{-19}$C while the m_0 was taken as 9.10939×10^{-31}kg. A condition that needed to be considered when selecting an applied magnetic field B_{app} value is shown in (3).

$$B_0 = \frac{2m_0\omega_s}{ne} \cdot \frac{1}{(1 - \frac{r_c^2}{r_a^2})} \quad [2]$$

$$B_{app} \leq B_o \quad [3]$$

The potential between the anode and cathode (the applied voltage) was determined as a value between limits that are defined by the Hartree Voltage (4) and Hull cutoff voltage (5). The Hartree voltage is the minimum DC voltage at which the electrons can reach the anode while influenced by an RF field for a given magnetic field while the Hull cutoff voltage is the maximum operating voltage for the magnetron [5]. These limits define the operating region of the magnetron [8]. When selecting the applied voltage, V_{app}, it had to meet the condition set in (6).

$$V_T = \frac{r_{an_{ir}}^2}{2}\left(1 - \frac{r_c^2}{r_{an_{ir}}^2}\right)\frac{\omega}{n}B_o - \frac{r_{an_{ir}}^2}{2}\frac{m}{e}\left(\frac{\omega}{n}\right)^2 \quad [4]$$

$$V_o = \frac{e}{8m}r_{an_{ir}}^2\left(1 - \frac{r_c^2}{r_{an_{ir}}^2}\right)B_o^2 \quad [5]$$

$$V_T < V_{app} < V_o \quad [6]$$

Table 2 outlines the design parameters that were calculated. The values shown are the results after adjustments were made to the initial physical dimensions. The changes made include increasing r_c to 4mm. These changes allowed the applied voltage and applied magnetic field to meet the conditions outlined in (3) and (6).

Table 2. Designed Parameters for an 8-Vane 5.8 GHz Magnetron

Design Parameter	Symbol	Value
Operating Frequency	f	5.8GHz
Number of Vanes	N	8
π-mode	n	4
Applied Magnetic Field	B_{app}	0.08T
Applied Voltage	V_{app}	3.5kV

2.3 Model creation

When creating a 3D model of the magnetron, considerations needed to be made with regards to the printing process. Processes such as DED or LPBF are not able to print overhanging structures without the addition of support material which can result in inaccuracies in the final product as manual post-processing of the print would be required. The best way to deal with this issue currently is to ensure that supports are minimised through proper design and orientation [9]. The research done in [10] showed that inclination angles have the strongest effect in predicting the manufacturability of a design as it was closely related to positional errors and surface quality. Thus inclination angles in the magnetron design were limited to 60° or 45°. The maximum thickness for any of the components modelled was 1.0mm which meant that several aspects of the magnetron needed to be increased in size. Given these constraints, the design of the magnetron needed to be elementary.

Autodesk Fusion was used to create a 3D model of the magnetron. The magnetron was separated into different segments to accommodate the constraints required by the 3D printing process. Hence the magnetron was separated into 11 segments: top section, bottom section, anode chamber, cathode, probes, antenna, antenna cap, steel cap, top ceramic seal, bottom ceramic seal and a vacuum port. The 3D models assembled together to form the magnetron can be seen in 6. Every part of the magnetron model was designed for 3D printing, but due to equipment constraints, the cathode structure, steel cap and the ceramic seals would not be printed in this paper. The tungsten filament can be created through additive manufacturing processes through wire extrusion and mechanical winding. Steel can be printed using DED or L-PBF and Alumina can be printed using Stereolithography as shown by [11], but at the time, these were not an accessible options.

Fig. 6. 3D Model of the Assembled Magnetron

The simulation process, did not require the full magnetron assembly given the tests that were run. The anode and cathode were the only components required as well as a model of the vacuum space within the magnetron. The model that was used within the simulation environment is shown in 7.

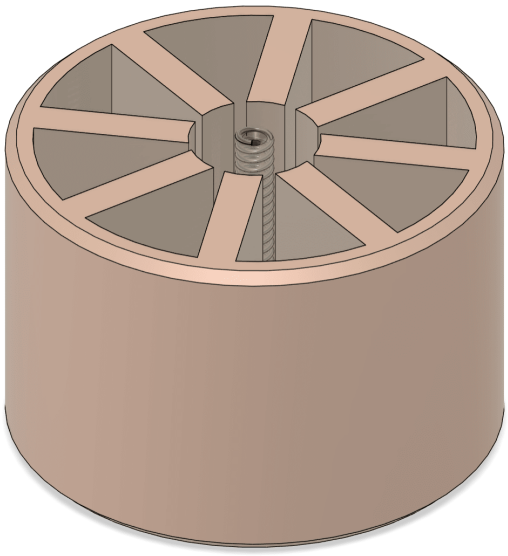

Fig. 7. 3D Model of the Internal Magnetron Structure

3. Magnetron material simulation

CST Studio Suite is a software package that is used for 3D electromagnetic analysis. It contains CST Particle Studio which can be used for the analysis of magnetrons. Eigenmode Analysis and Particle Tracking are two simulations that are performed on magnetrons typically. These simulations were chosen to evaluate the effectiveness of three different materials, perfectly electric conducting (PEC) material, copper and aluminium. The PEC material is a default material provided by CST Studio Suite and was used to emulate perfect operating conditions for the magnetron. The results obtained from the simulations for this material were used as a baseline to determine how well the copper and aluminium magnetrons operated. The second material evaluated was copper which was chosen as it is the material that is commonly used for commercial magnetrons. Aluminium was the final material evaluated which was selected as it is a material that can be found in lunar environments.

3.1 Eigenmode analysis

Eigenmode Analysis is used to determine the resonant modes and the electromagnetic field patterns of the magnetron [8]. The main goal of using an Eigenmode solver for Eigenmode Analysis is to verify the dimensions chosen for the magnetron to ensure that it operates in π-mode. The dimensions for the anode height, inner anode radius and vane thickness cannot be found using formulas or equations and must be found through an iterative process in the Eigenmode simulation process [8]. Two different solvers can be used for Eigenmode Analysis: Advanced Krylov Subspace (AKS) or Jacobi-Davidson Method (JDM). The AKS solver uses a predefined frequency interval while the JDM solver has no frequency limit but has a much larger solving time which is not always necessary depending on the scale of the magnetron [8].

The Eigenmode Analysis in this project makes use of the eigenmode solver in CST Studio Suite. In order to reduce the solver time an AKS solver was used for the analysis. Since the eigenmode analysis is a cold test for the magnetron the boundaries were set so that the tangential electric field was 0 in all boundary directions. In CST Studio Suite, the anode and cathode were removed from the simulation environment leaving behind the vacuum filled interaction space for the Eigenmode solver. The frequency range for the simulation was then set as 0 to 12GHz. The background was set as the the material that was being evaluated (PEC, Copper or Aluminum). A Hexahedral mesh type was chosen along with 8 modes since an 8 vane magnetron was being simulated.

Fig.8. shows the electromagnetic field patterns of each magnetron type after the Eigenmode Analysis. The electromagnetic field patterns for all three magnetrons indicate that they are all operating in π-mode as there is a 180° phase difference between the vanes. This is confirmed by the alternating directions of the vectors in the vane cavities for each magnetron. The frequencies for the PEC, Copper and Aluminum were 5.036GHz respectively. This shows that the Copper and Aluminium both worked very well to maintain the π-mode operations of the magnetron at a value that is relatively close to the designed 5.8GHz operating frequency.

The Surface Current patterns for each magnetron is shown in Fig.9. From these results, very little difference in the concentration of the pattern can be seen between the PEC magnetron and the Copper and Aluminum. This is to be expected as both Copper and Aluminum are considered lossy metals and so there would be resistive losses. The Aluminum Magnetron has the lowest surface current density of the three materials, but it is not a drastic difference. This indicates that while it may not be as efficient as Copper, it is still able to perform as needed in the capacity of a magnetron.

3.2 Particle tracking

CST Studio Suite offers a Particle Tracking Solver as part of CST Particle Studio. Unlike the Eigenmode Analysis, the anode and the cathode remained in the simulation for the particle tracking. The materials for both components were varied between PEC, Copper and Aluminium

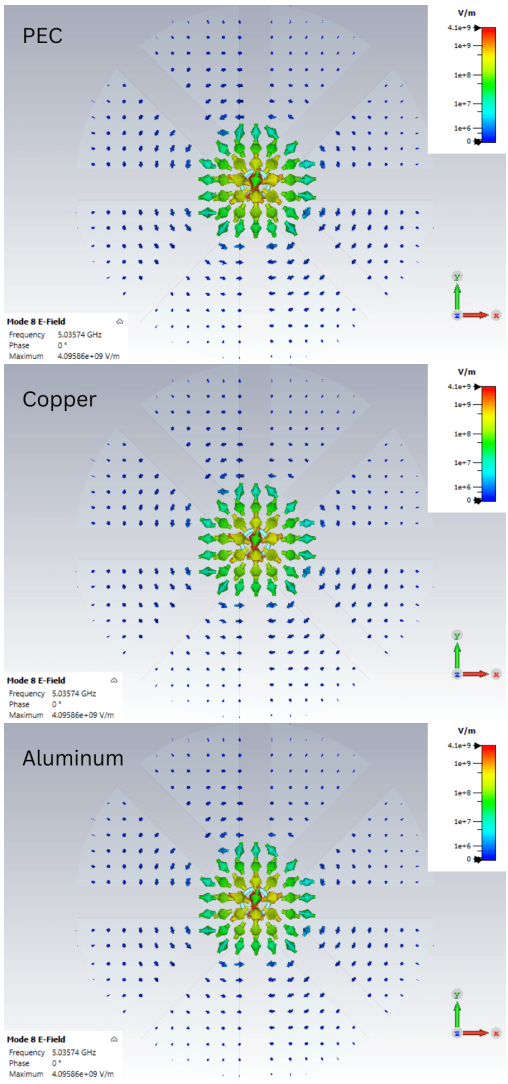

Fig. 8. Electromagnetic Field Patterns for a PEC, Copper and Aluminum Magnetron

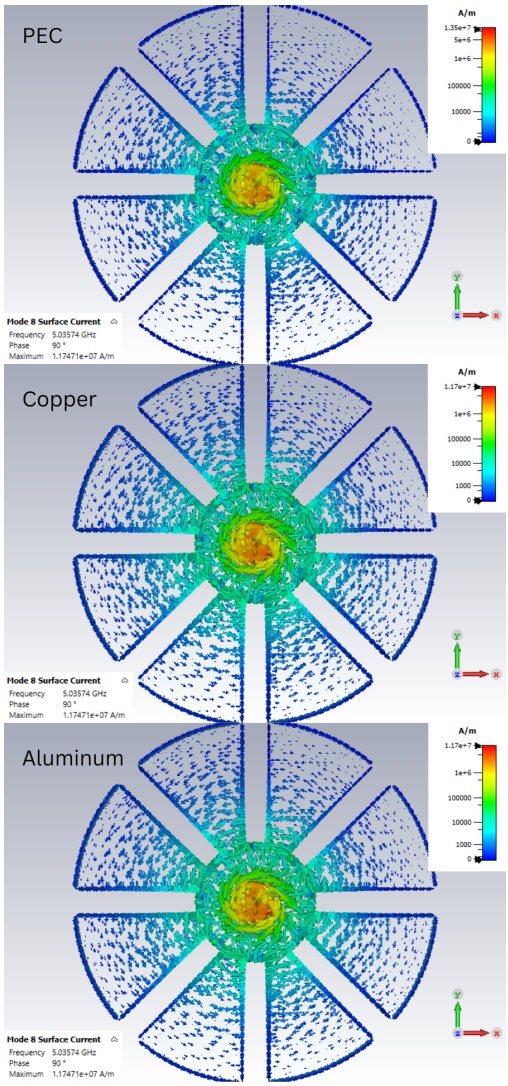

Fig. 9. Surface Current Patterns for a PEC, Copper and Aluminum Magnetron

while the background was set to Normal which emulates vacuum conditions. The frequency remained at a range from 0 to 12 GHz and the boundary conditions were set to be open in all directions except for the positive and negative Z directions where the magnetic (Ht = 0) condition was chosen in order to prevent the magnetic field from escaping the interaction space. The analytic source field was set to be 0.08 T based on the calculations. Two static potentials were defined in the simulation environment, where the anode was set to have a potential of V_{app} and the cathode had a potential of 0V. The cathode was set as the particle source with a fixed current emission model using a current of 10A.

Figure 10 shows the trajectory of all of the emitted electrons from the cathode while under the influence of an electromagnetic field. The maximum electron energy recorded for an electron sample was 3285.03eV, 3578.95eV and 3569.51 for the PEC, Copper and Aluminum magnetrons respectively. This indicated a minimal difference in the performance of each magnetron in terms of generating electrons with a high enough energy for generating microwaves.

11 shows the motion of an individual electron sample in each Particle Tracking Simulation for the different magnetrons.

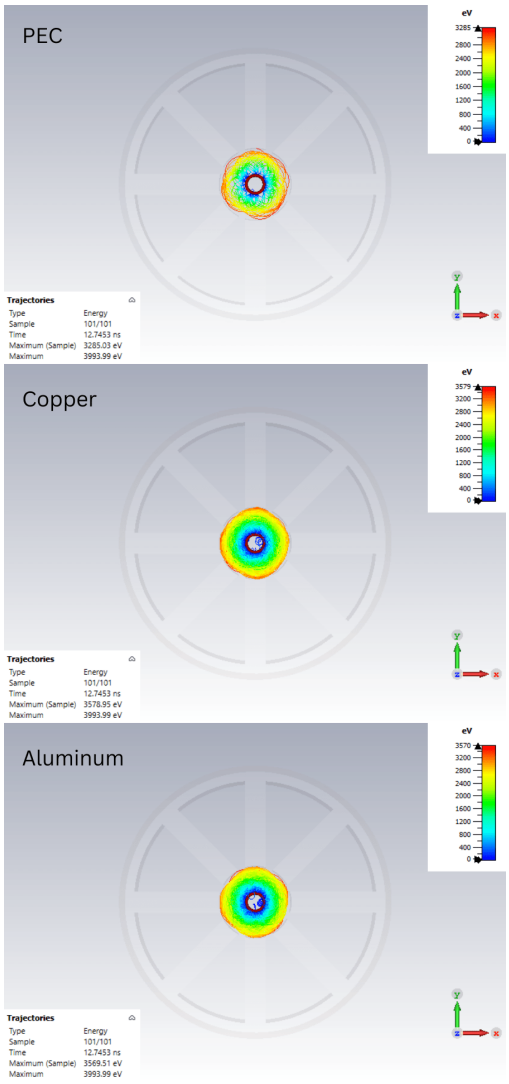

Fig. 10. Trajectory of All Electrons Emitted from the Cathode of the Magnetron Design

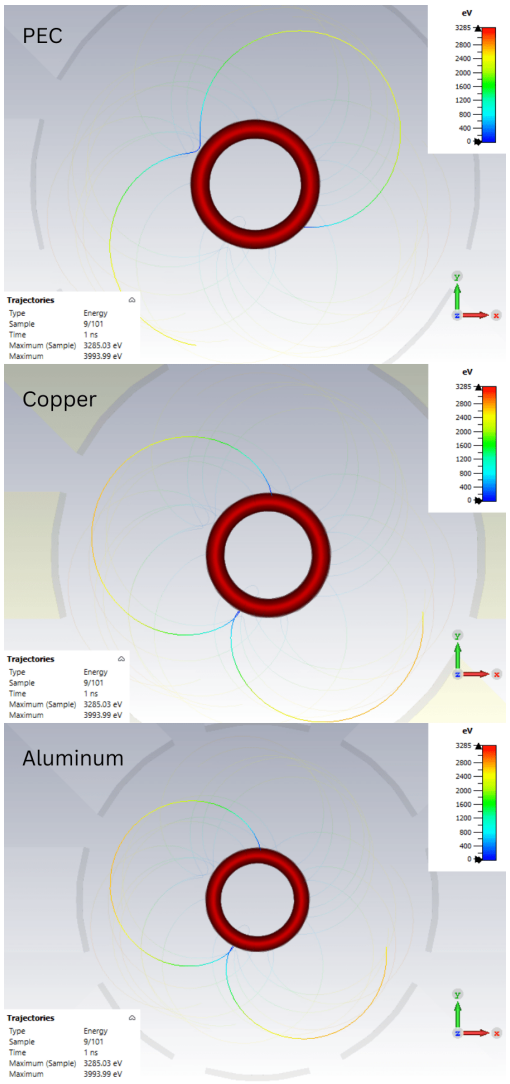

Fig. 11. Trajectory of a Single Electron in a PEC, Copper and Aluminum Magnetron

4. 3D printing process

After the simulation procedure to verify the design of the magnetron, the model was ready to be 3D printed. The two metal 3D printing processes were considered for the production of the magnetron were DED and L-PBF. DED is a 3D printing process in which a feedstock material in the form of powder or wire is delivered to a substrate that also has a focused energy source, thus forming a melt pool which continuously has material deposited, layer by layer[12]. DED is typically used with metal alloys and has decreased geometrical capabilities, requiring extensive machining operations for parts to achieve the appropriate shapes [13]. L-PBF uses a selective laser melting (SLM) machine and allows for more complex parts to be manufactured without additional post-processing needed and minimal geometric restrictions [14]. Hence, for the magnetron, L-PBF was selected as it would permit the complex shapes of the magnetron to be printed without the need for any post-processing.

We developed different detailed Computer-Aided Design (CAD) models for each of the magnetron parts as a blueprint for the final printed part. We considered different factors for our design such as the precision and tolerance each part and the use of any necessary support structures as overhangs for complex features such as the hole use for the vacuum inlet located at the anode bottom. Once

the parts were finalized, they were imported into a slicing software where the parts were oriented and positioned on the build plate. The software sliced out parts into a total of 1383 layers. The Cu14500 powder was loaded into the machine, and everything was prepared for the print. The print took a total of 25hours. The parts were cut off the plate by manual sawing and the surfaces were smoothened out to remove any sharp edges.

The L-PBF printing was carried out at the University of Waterloo's Multi-Scale Additive Manufacturing Lab using an EOS M290 Printer. With the help of the MSAM team at Waterloo, the model of the magnetron was refined to ensure the best printing results. A C14500 alloy from Metal Powder Works was chosen for the Copper print. This is a Copper Tellurium alloy that has similar conductivity to pure copper with added strength benefits allowing for better manufacturability [15]. C14500 also has a high melting point and will be able to withstand the high temperatures required by the Cathode for thermionic emission.

Before printing, different factors for the design such as the precision and tolerance of each part and the use of any necessary support structures as overhangs for complex features such as the hole use for the vacuum inlet located at the anode bottom. Once the parts were finalized, they were imported into a slicing software where the parts were oriented and positioned on the build plate. The software sliced out parts into a total of 1383 layers. The Cu14500 powder was loaded into the machine, and everything was prepared for the print. The print took a total of 25hours. The parts were cut off the plate by manual sawing and the surfaces were smoothened out to remove any sharp edges. The parts shown in Fig. 12 were the result of the L-PBF process using C14500. The parts were printed with minimal imperfections.

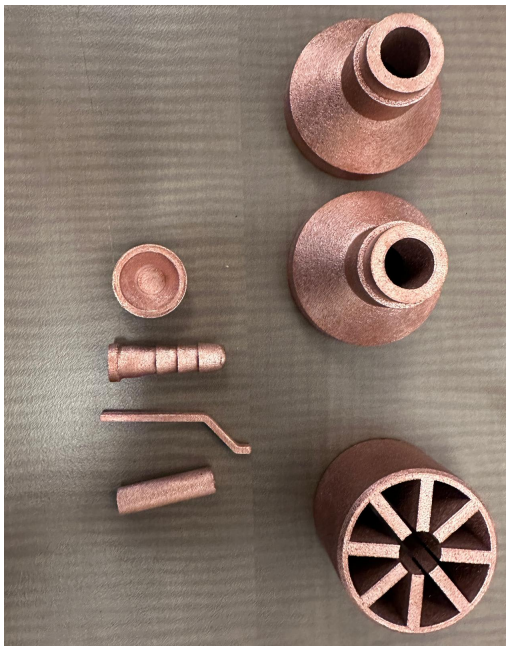

Fig. 12. 3D Printed Parts of the Magnetron

5. Future work

The next steps in this research is to join the parts of the magnetron through either brazing or soldering, and evacuate the structure to a high level vacuum level between 10^{-5}Torr and 10^{-9}Torr. Ideally, a vacuum level of 10^{-7}Torr would be achieved within the magnetron. Once the magnetron is assembled, the vacuum holding capabilities of the material can be tested. If the 3D printed material is capable of holding a high vacuum level, the power output and frequency analysis can be tested and compared to the performance of a commercial level magnetron. If proper magnetron operation is achieved for the Copper printed magnetron, an Aluminum magnetron can then be modelled and printed and the same procedure can be executed.

6. Conclusion

This paper showed the design, simulation and printing process of a 5.8 GHz 8-vane magnetron. This was done by disassembling a commercial magnetron to use as a reference point followed by design calculations which allowed the magnetron to be designed for the specific use case of SPS systems. An initial model was then created based on the design calculations and this model was imported to CST Studio Suite to simulate how different materials affected the magnetron performance. PEC, Copper and Aluminum were the materials evaluated using Eigenmode Analysis and Particle Tracking. The results of these analyses showed that Aluminum is a viable alternative to Copper for magnetron performance. Once the magnetron design was verified by simulation, a 3D print was made using L-PBF printing methods and C14500 alloy. The 3d print was successful with minimal imperfections. The parts of the magnetron can now be joined and tested to determine whether a functional magnetron can be 3D printed.

Acknowledgements

We would like to express our sincere gratitude to Metal Powder Works for generously providing the Cu powder used for the 3D printing process. We would also like to deeply thank Prof. Mihaela Vlasea for her invaluable support allowing the 3D print to happen. Additionally, we would like to extend our appreciation to Zachariah Mears, whose assistance in verifying the feasibility of 3D print-

ing our designs was essential to the success of this project. Finally, we would like to thank Xavier Walls-Perez for all of his support in the 3D Printing Process and for the time spent corresponding on our behalf with the MSAM team.

References

[1] A. Ellery, "Solar power satellites for clean energy enabled through disruptive technologies," in *Proc 23rd World Energy Congress (Award Winning Papers)*, 2016, pp. 133–147.

[2] P. Glaser, "An overview of the solar power satellite option," *IEEE Transactions on Microwave Theory and Techniques*, vol. 40, no. 6, pp. 1230–1238, 1992. DOI: 10.1109/22.141356.

[3] H. Matsumoto and K. Hashimoto, "Report of the ursi inter-commission working group on sps and appendices," in *White Paper on Solar Power Satellite (SPS) Systems for the General Assembly and Scientific Symp. of Int. Union of Radio Science< http://www. ursi. org>, URSI, Ghent, Belgium*, 2006.

[4] A. Leggieri, F. Di Paolo, and D. Passi, "Key-holes magnetron design and multiphysics simulation," in *Proc. of COMSOL Conference 2013*, 2013, pp. 69–72.

[5] R. G. Carter, *Microwave and RF Vacuum Electronic Power Sources* (The Cambridge RF and Microwave Engineering Series). Cambridge University Press, 2018.

[6] C.
bibinitperiod P. Industries. "Cpii.com." [Accessed 29-03-2024]. (2020), [Online]. Available: https://www.cpii.com/docs/related/2/MAG%20TECH%20ART.pdf.

[7] G. B. Collins, *Microwave Magnetrons* (Massachusetts Institute of Technology Radiation Laboratory Series). 1948.

[8] T. Isenlik and K. Yegin, "Tutorial on the design of hole-slot-type cavity magnetron using cst particle studio," *IEEE transactions on plasma science*, vol. 41, no. 2, pp. 296–304, 2013.

[9] G. Piscopo, A. Salmi, and E. Atzeni, "On the quality of unsupported overhangs produced by laser powder bed fusion," *International Journal of Manufacturing Research*, vol. 14, no. 2, pp. 198–216, 2019.

[10] A. Jones, M. Leary, S. Bateman, and M. Easton, "Effect of surface geometry on laser powder bed fusion defects," *Journal of Materials Processing Technology*, vol. 296, p. 117 179, 2021.

[11] S. Mamatha, P. Biswas, P. Ramavath, D. Das, and R. Johnson, "3d printing of complex shaped alumina parts," *Ceramics International*, vol. 44, no. 16, pp. 19 278–19 281, 2018.

[12] D. Svetlizky *et al.*, "Directed energy deposition (ded) additive manufacturing: Physical characteristics, defects, challenges and applications," *Materials Today*, vol. 49, pp. 271–295, 2021.

[13] M. Hoffmann and A. Elwany, "In-space additive manufacturing: A review," *Journal of Manufacturing Science and Engineering*, vol. 145, no. 2, p. 020 801, 2023.

[14] W. Abd-Elaziem *et al.*, "On the current research progress of metallic materials fabricated by laser powder bed fusion process: A review," *Journal of Materials Research and Technology*, vol. 20, pp. 681–707, 2022.

[15] C. D. A. Inc. "C14500." [Accessed 29-03-2024]. (2024), [Online]. Available: https://alloys.copper.org/alloy/C14500.